Erschienen in: Proceedings of the 28th European Photovoltaic Solar Energy Conference and Exhibition (EU PVSEC 2013) ; Paris, France ; conference 30 September - 04 October 2013. - München : WIP, 2013. - S. 1512-1517. - ISBN 3-936338-33-7
https://dx.doi.org/10.4229/28thEUPVSEC2013-2BV.3.56

DEFECT CHARACTERIZATION AND INVESTIGATION OF RST-SILICON RIBBON WAFERS

Philipp Keller[1], Annika Zuschlag[1], Philipp Karzel[1], Fabrice de Moro[2], Giso Hahn[1]
[1] University of Konstanz, Department of Physics, 78457 Konstanz, Germany
[2] Solarforce, 1 rue du Dauphin, 38300 Bourgoin-Jallieu, France

ABSTRACT: The electronic and material properties of Ribbon on Sacrificial Template (RST) silicon wafers are investigated in this work. Like all multicrystalline wafers, RST wafers exhibit many grain boundaries, impurities and other crystal defects. The understanding of these defects and their influence on material quality is an important part of the characterization of solar cell material. The minority carrier lifetime of RST samples after $POCl_3$ diffusion and SiN_x:H_y hydrogenation is obtained by quasi-steady state photo conductance decay measurements. The distribution of lifetime on a wafer and the influence of grain boundaries and bulk resistivity are studied via photoluminescence imaging. Local defects, revealed with the help of a defect etch, are qualitatively correlated to lifetime values. The crystal orientation and the type of the grain boundaries between the different grains was measured with electron back scatter diffraction. The most common grain boundaries in the investigated area are of coincidence type Σ3. SiC particles on the silicon surface as residues of ribbon casting are studied by scanning electron microscopy. A focused ion beam cut through a SiC particle reveals the interface structure between these particles and the silicon wafer surface.
Keywords: RST, ribbon silicon, cost reduction, defects, defect density, lifetime, grain.

1 INTRODUCTION

The Ribbon on Sacrificial Template (RST) technology can pave the way for reducing silicon wafer and module costs. The RST technique, formally known as ribbon against drop (RAD) [1], belongs to the family of silicon ribbons [2]. Advantages of the ribbon technologies are that no kerf-losses occur and energy can be saved, as no energy-consuming ingot growth is needed. Also, the ribbon wafers in the RST process can be grown very thin (down to 50 µm). This in total leads to reduced energy and material costs which can directly have an effect on a shortened energy payback time of a module. RST wafers, as well as all multicrystalline (mc) wafers, exhibit grain boundaries, impurities and other crystal defects. The understanding of defects and their influence on cell efficiency is an important part of the characterization of solar cell material. This can lead directly to an adjustment and improvement of silicon ribbon production and cell processing.

2 EXPERIMENTAL

For this purpose lifetime samples are processed on 5x5 cm² RST wafers. The effective minority-carrier lifetime τ_{eff} is measured by quasi-steady-state photoconductance decay (QSSPC) [3]. Its distribution and the influence of grain boundaries are investigated with the help of photoluminescence imaging (PLI) [4]. Whereas various investigations have been performed on defect clusters and performance limitation for standard mc wafers (e.g. by Sopori et al. [5]), there are almost no corresponding analyses of RST wafers. The lifetime samples are etched in a defect etch solution suggested by Sopori [6] to reveal the crystal structure, grain boundaries and defects. Local defects are qualitatively correlated to spatially resolved measurement of τ_{eff} from QSSPC calibrated PL maps [7]. With the help of electron back scatter diffraction (EBSD) [8] the crystal orientation and the type of the grain boundaries between the different grains is measured. Thus the influence on the minority carrier lifetime can be estimated.

Impurities and SiC particles formed due to the unique RST process are observed and analyzed with a scanning electron microscope (SEM). The elemental composition of some particles is determined by energy dispersive X-ray (EDX) spectroscopy. The interface of a particle is investigated after a focused ion beam (FIB) cut through a characteristic particle.

3 RST RIBBON MATERIAL

The RST process belongs to the family of silicon ribbon technologies and represents a method of fast and kerf-loss free wafer casting [9]. It is based on direct crystallization of molten silicon onto a soft carbon substrate which is pulled vertically through a silicon melt. The carbon carrier is coated by a thin layer of pyrocarbon which makes it wetable by silicon and resistant to erosions by molten silicon [10].

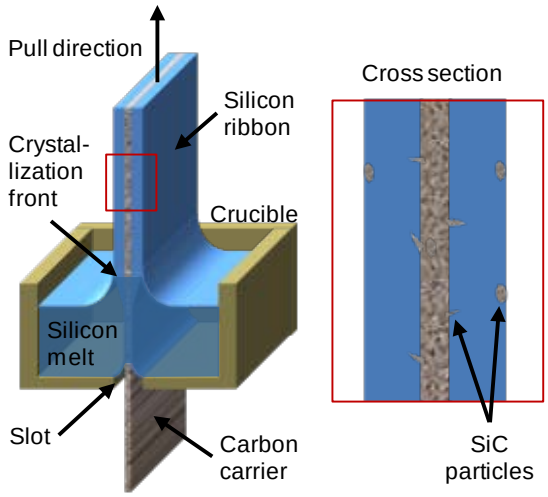

Figure 1: Schematics of the RST casting process (left). A carbon based carrier is pulled through molten silicon which crystallizes on the carrier surface. The cross section through the silicon-carbon-silicon triple layer (right) is shown.

A schematic of the RST casting process is shown in Fig. 1.Two wafers are gained after removing the substrate by a subsequent high-temperature burn-off step. The technique allows wafer thicknesses down to about 50 µm and high wafer throughput rates proportional to the pull speed in the order of 5-10 cm/min [1]. This is about 2-4 times faster than the speed of the comparable EFG (Edge-defined Film-fed Growth) process [11]. The silicon surface predominantly yields a (011) orientation and the grains grow elongated in the pulling direction of the carbon carrier [10]. The wafers which are investigated in this work are produced by the company Solarforce in France which successfully applies the RST technology.

4 LIFETIME STUDIES

Material properties are investigated by the analysis of lifetime samples.

4.1 Influence of the base resistivity

In the lifetime study the influence of the base resistivity on τ_{eff} of RST wafer is investigated. Thus different wafers with projected base resistivity of 1.5-5.0 Ωcm and initial thickness of 90-95 µm were produced at Solarforce. Other ribbon casting parameters like the burn-off time, the pulling speed and the thickness d of the ribbon were within the same range. Tab. 1 gives an overview of the elemental parameters of the different batches of wafers. T_b is the burn-off temperature of the furnace where the wafers are separated from the carbon carrier. The wafers were laser cut from a long ribbon at a certain position which is also given in Table I in meters.

Table I: Parameters of the RST process of the different batches of wafer.

Batch	T_b	Pos. m	$\rho_{approx.}$ Ωcm	d µm
RST1	high	9	1.5	90
RST2	high	21	3	90
RST3	low	22	3	90
RST4	low	10	3.5	80
RST5	low	5	5	95
RST6	low	12	5	80

In total 36 5x5 cm^2 wafers are processed to lifetime samples. All samples were treated in a chemical polishing (CP) solution containing HF, HNO_3 and CH_3COOH to remove the defect-rich surface. To remove metal impurities which have a strong influence on τ_{eff}, a phosphorous gettering step was performed. Therefore a standard 55 Ω/□ $POCl_3$ emitter diffusion was carried out in an industrial-type tube furnace. The phosphorous silicate glass (PSG) and the emitter were removed in HF and in a CP subsequently. The measured τ_{eff} is affected by the recombination of the minority-carriers at the sample's surface. To minimize the influence of the surface recombination, the samples were passivated by 30 nm thick Al_2O_3 layers realized by plasma-assisted atomic layer deposition (PA-ALD) in an Oxford Instruments tool (FlexAL). Afterwards τ_{eff} was determined using QSSPC measurements. The lifetime was evaluated at an excess carrier density of $1 \cdot 10^{15}$ cm^{-3}. Fig. 2 shows τ_{eff} of the RST samples versus their base resistivity ρ which was also determined by the QSSPC method.

One conspicuous difference are the relatively high lifetime values between 9.0-14.5 µs of the samples with ρ<1 Ωcm (Fig. 2, RST1) while all other samples with higher base resistivity do not exceed 13 µs.

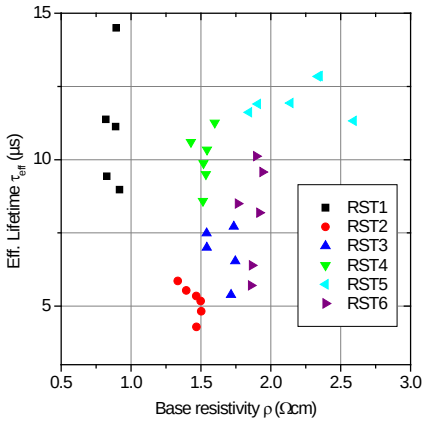

Figure 2: Effective lifetime of P-gettered RST wafers versus their base resistivity. Both measurements were determined by the QSSPC method.

This can be issued to the pyrocarbon capping layer of the carrier which was used for this specific ribbon casting. A high capping quality leads to a lower SiC particle density and thus to higher lifetime values. The SiC particles will be discussed later on in section 5. Except for the results of batch RST1, a clear trend of τ_{eff} versus ρ is visible. The samples from batch RST2 show an average resistivity of ρ_2=1.4 Ωcm and the lowest average lifetime of τ_2=5.2 µs. Casting batch RST4 has a comparable average resistivity of ρ_4=1.5 Ωcm, but nearly a doubled average lifetime of τ_4=10.1 µs. Having a look at Table I one can see that RST4 had a lower burn-off temperature than RST2. Higher burn-off temperatures can lead to lower material quality since several defects like dislocations and grain boundary decoration are temperature induced. The effect of burn-off temperature is currently under further investigation. Another point is the position of the wafers on the RST ribbon. RST4 was cut out earlier from the ribbon (Pos. 10 m) than RST2 (Pos. 21 m). This is possibly an effect of the casting order where the material quality changes with the impurity concentration in the silicon melt. RST3 with τ_3=6.8 µs at ρ_3=1.7 Ωcm and RST6 with τ_6=8.1 µs at ρ_6=1.9 Ωcm are in good agreement with the expectations. The highest lifetime values are observed on RST5 with τ_5=12.1 µs at ρ_2=2.2 Ωcm. However, an optimization of the bulk resistivity in terms of total average lifetime does not necessarily lead to the best solar cell results. Former investigations of RST on solar cell level led to the assumption that lower bulk resistivity results in higher solar cell performance [12].

4.2 Influence of hydrogenation

Hydrogen can have a strong influence on the average bulk lifetime of the minority-carriers of multicrystalline and especially ribbon silicon wafers (e.g. [9, 13]) and can be explained with the passivation of defects by atomic H. RST wafers exhibit multiple defects and a very high density of grain boundaries (GB) whereof most of them are twin boundaries. Thus the influence of hydrogen should be beneficial, if the defects can be passivated by

atomic H. RST lifetime samples are processed in the same way as described in section 4.1. But instead of a standard industrial 55 Ω/□ $POCl_3$ emitter, an emitter with 90 Ω/□ was applied. This emitter is also used for RST wafer cell processing. The source for hydrogen is a H-rich SiN_x:H_y layer deposited in a plasma-enhanced chemical vapor deposition (PECVD) process. The prepared samples are fired in an industrial belt furnace with peak temperature above 700°C. This leads to a diffusion of H into the silicon bulk. Fig. 3 shows the PL images of a RST wafer after P-gettering (left) and another RST wafer after P-gettering and subsequent hydrogenation. The RST wafers are too thin to allow for multiple processes including CP on one single sample. Therefore the measurements after certain processing steps are done on different RST wafers. The PL images are calibrated with the values of the corresponding QSSPC measurements at the excess charge carrier density Δn corresponding to the generation rate of the PL measurement. Δn was close to $1 \cdot 10^{14}$ cm^{-3} according to 1 sun illumination and thus the operating condition of a solar cell.

Table II gives the lifetime values τ_{QSSPC} of these two samples at $\Delta n = 1 \cdot 10^{14}$ cm^3 measured via QSSPC, the arithmetic average value τ_{PL} determined by the PL image and the harmonic average value $\tau_{PL,\ harm.}$. It has been shown by Wagner et al. [14], that for inhomogeneous lifetime distribution, the harmonic aveerage value is more adequate for solar cell simulations.

Table II: Average effective lifetimes from the two RST samples measured by QSSPC and PL at a MCD of 10^{14} cm^3.

Sample	τ_{QSSPC} µs	$\tau_{PL,\ arith.}$ µs	$\tau_{PL,\ harm.}$ µs
RST after $POCl_3$	4.3	3.8	3.2
RST after $POCl_3$ + H	6.2	5.7	5.1

The elongated grain structure with relatively good lifetimes is clearly visible on both samples of Fig. 3. The GBs with poor lifetimes cross through the bulk in a fiber-like structure. Areas with τ_{eff}<2 µs are marked in black. A comparison of the two different samples reveals the beneficial effect of hydrogenation on τ_{eff}.

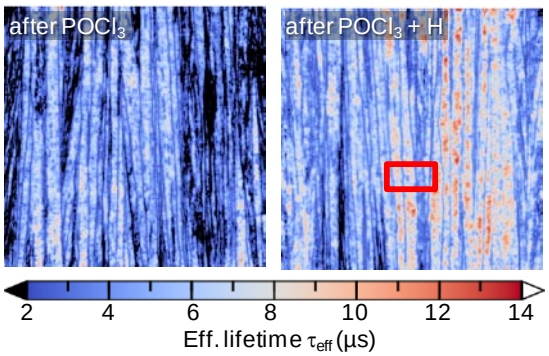

Figure 3: PL image of 5x5 cm^2 RST wafers after $POCl_3$ gettering (left) and after $POCl_3$ gettering and hydrogenation. Lifetime calibration is performed by QSSPC measurement data.

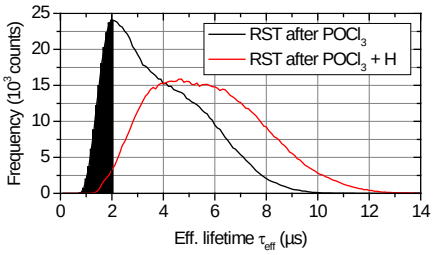

Figure 4: Distribution of lifetime of the samples shown in Fig. 3. Hydrogenation leads to a broadening of the distribution and a shift to higher values.

After hydrogenation (Fig. 3, right) there is nearly no area or GBs with τ_{eff} <2 µs. Although it is a question of two different wafers it can be concluded that many defects in RST wafers can be passivated by H. The histograms in Fig. 4 show the distribution of τ_{eff}. The distribution is similar for all measured lifetime samples and characteristic for these kinds of RST wafers. After $POCl_3$ gettering (Fig. 4, black line) the samples exhibit a distinct peak in the lifetime distribution around 2 µs. The black area below the distribution function represents the black areas in Fig. 3 with τ_{eff} <2 µs. After hydrogenation the distribution is broadened and the characteristic peak disappears. Most of the lifetime values are shifted to higher values.

4.3 Influence of grain boundaries and defects

Not all defects and GBs can be sufficiently improved by hydrogenation in terms of lowered recombination of minority-carriers. To reveal the crystal structure, grain boundaries and defects, the lifetime samples were etched in a defect etch solution suggested by Sopori [6]. Because of the disturbed crystal structure the etching rate is higher at defects. This results in a contrast visible at high resolution optical microscopy images of the etched samples. Hence it is possible to qualitatively correlate the defect structure with the lifetime map of the PL measurements and to draw conclusions from the passivation mechanisms of H.

Former investigations on mc-Si wafers dealt with the passivation efficacy of hydrogen at GBs of different coincident site lattice (CSL) types [15-18]. The CSL type of the GBs can be determined if the crystal orientation of neighboring grains is known. Therefore, electron back scatter diffraction (EBSD) measurements [8] with a scanning electron microscope (SEM) are carried out on a small area of 0.3x6.5 mm^2 on a RST sample after P-gettering and hydrogenation. The sample properties are described in section 4.2 and the region of interest is marked by the red lined box in Fig. 3. The EBSD scan is performed within this region which is shown in Fig. 5b) in detail. Here the PL image, the optical microscopy image of the revealed defects and the CSL GB types are simultaneously shown and correlated.

The defect etch reveals a relatively high line density of GB in the order of 10^5 m^{-1}, which is 1 GB per 10 µm. An impurity inclusion shown at Fig. 5b) ① can lead to a disturbance of the crystal growth. This is indicated by the discontinuity of the almost parallel GBs (arrow in Fig. 5b)).

The EBSD measurement shows: the predominant part of GBs is of type Σ3 which do not all visibly appear in the PL image of this sample. This accounts for the fact that Σ3 grain boundaries are not the main reason for limitation of

lifetime in RST wafers which is also shown for mc wafers by Karzel et al. [19]. On the investigated area shown in Fig. 3c) the by far predominant type of GB is Σ3 (marked in red), whereas the other types indicated by the arrows are far less frequent: Σ9 (violet), Σ27a (green).

A linescan of τ_{eff} which cuts through the middle of the EBSD area is shown in Fig. 5a). The variance of the lifetime (3-9 µs) can solely be explained by the different types of CSL GBs. The orange outlined area of Fig. 5b) contains high (>8 µs) and poor (<4 µs) lifetime values. This is visible in the τ_{eff} line scan between a distance of 3.2-4.4 mm which is framed by the orange lines. Fig. 5c) shows the magnification of the orange box. At the area around ② a high defect density inside the different grains occurs. These defects show up as little etch pits after a defect etch and are probably linked to dislocations in the silicon crystal. Although this area is dominated by Σ3 GBs, the lifetime is rather poor. The underlying PL image has a resolution of 50 µm/pixel and can thus not give the same resolution as the optical microscopy image or the EBSD map with a resolution of 3 µm/pixel. But still the tendency of lower lifetimes at higher defect densities is recognizable. The area around ③ is also dominated by Σ3 GBs, but shows barely no etch pits. The recombination of minority carrier is reduced in this area leading to higher

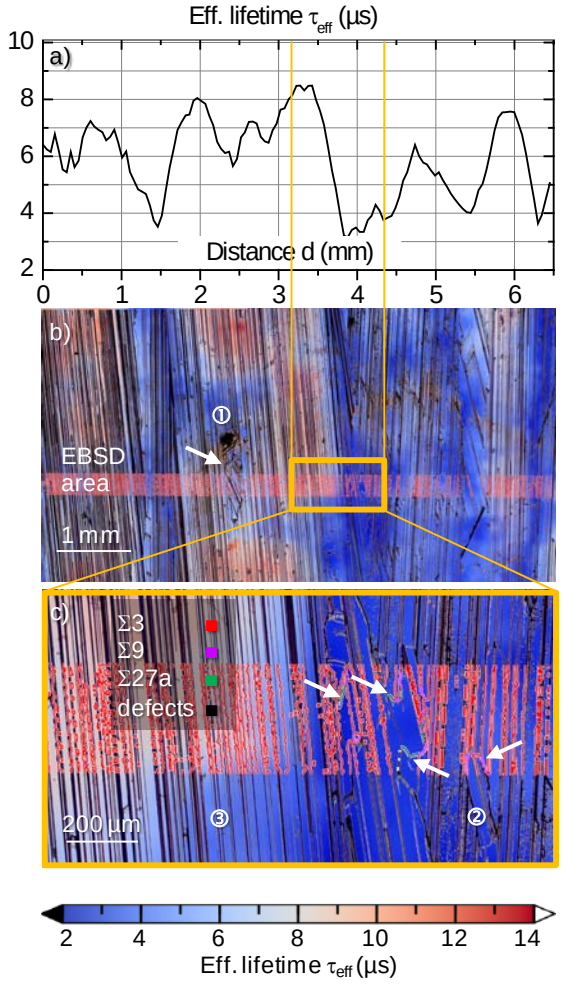

Figure 5: a) Line scan of the effective lifetime. The region of interest is marked in Fig. 3 by the red box. b) Correlation of PL image, crystal structure and CSL GB type. c) Magnification of the correlation.

τ_{eff} values. Other CSL grain boundary types apart from Σ3 appear at the interface of the two different main grain orientations (indicated by region ② and ③ in Fig. 5c). The arrows point at some exemplary interface positions where Σ9 and Σ27a GBs can be found. Although the etch pit density is low at the aforementioned interface, τ_{eff} does not improve very much after hydrogenation. This means that the recombination activity of GBs with CSL indexes higher than Σ3 cannot be fully compensated by H.

5 SURFACE STUDIES

The rear surface of the RST wafer (being in contact with the carrier during crystallization) exhibits different types of impurities which are macroscopic and cannot be fully removed by chemical polishing. This leads to the assumption that the impurities are grown in the silicon bulk.

The growth of silicon ribbons in combination with carbon casting parts results in the formation of silicon carbide (SiC) particles at the silicon carbon interface. Thus the crystal growth is accompanied by the inclusion of some of these SiC particles. This was also observed on ribbon wafers of the related EFG process [20]. One source for the formation of SiC particles is the crucible and the crucible slot where the particles can freely be transported in the molten silicon and can be included in the growing ribbon. Another source of SiC particle formation appears directly between the carbon carrier surface and the molten silicon. A discontinuity in the pyrocarbon capping layer of the carrier can lead to a local reaction of silicon and carbon with an attendant diffusion of carbon into the growing ribbon and SiC crystal formation. The same reaction can take place vice versa when silicon diffuses into the carbon carrier.

5.1 SEM and EDX analyses

The rear surface of a RST wafer was examined with a SEM after chemical polishing (removal of about 10 µm silicon). Fig. 6 shows different types of impurities which are identified on the surface. A typical round shaped 0.3x0.2 mm^2 particle is shown in Fig. 6a). The elemental compositions which are determined by an EDX measurement are summed up in Table III. The rounded particle holds a high silicon content (>85%) with a small carbon percentage (<15%) at position ①. It is assumed that these kinds of particles are left-overs from the soft carbon carrier. By removing the carbon carrier in a high temperature burn-off step, parts of the carbon which stick to the bulk remain on the silicon surface. Another kind of impurity, observed on the round shaped particle, is not directly connected with the wafer. An EDX analysis at position ② revealed a high concentration of carbon (>56%). The indicated silicon content may be caused by the background. Probably these carbon impurities are direct residuals of the carrier which are electro-statically bound to the surface or freed by the CP. The relatively high content of oxygen (~30%) may come from the burn-off step under oxygenic atmosphere which reacts with the carbon.

Some particles show the typical hexagonal crystal structure of SiC [20] as can be seen in Fig. 6b). The EDX measurement on a spot and a small area on this kind of SiC particle (③ and green area) reveals a silicon content of >66% and a carbon content of around 30%. This corresponds to a relation of Si:C=2:1.

Table III: Elemental composition of impurities on the surface measured by EDX.

Measurement point in Fig. 6	Si mass%	C mass%	O mass%
SiC particle, ①	85.4±0.9	14.6±0.9	-
Carbon particle, ②	14.6±0.3	56.2±0.9	29.2±0.8
SiC particle ③	66.4±1.2	32.6±1.2	1.0±0.4
SiC particle ③ area	70.2±1.3	27.7±1.3	2.1±0.5

5.2 Bonding structure of SiC particles

The character of the SiC particle bonding to the silicon surface and the depth of the SiC crystal in the silicon bulk is investigated by a SEM imaging of a cross section of a typical SiC particle. A 30 µm deep FIB cut through a characteristic SiC particle is performed. In Fig. 6b) the FIB cut is denoted by a red line.

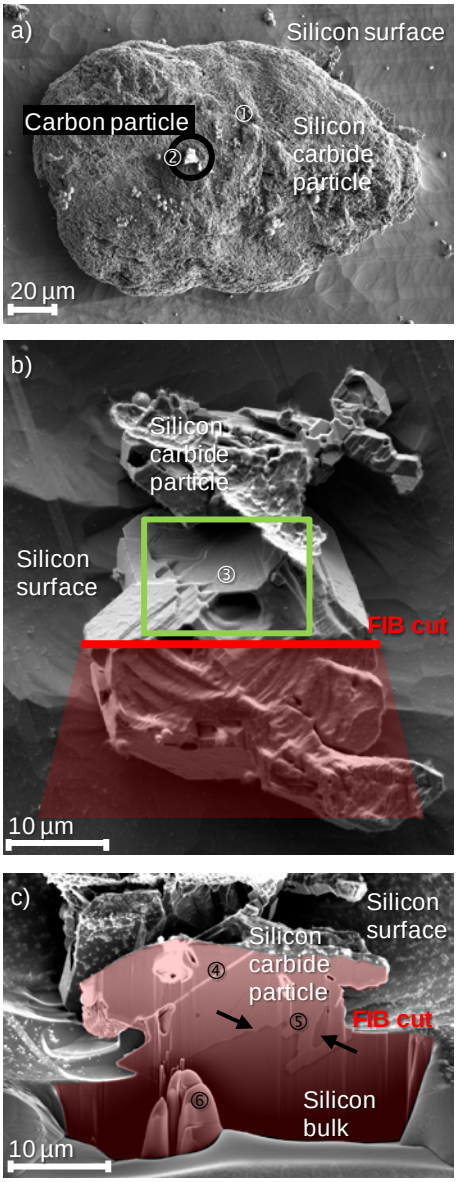

Figure 6: SEM images of different particles, observed on the RST wafer surface: a) typical round shaped SiC particle with a small carbon piece on top. b) SiC crystal with typical hexagonal growth which is bonded to the surface. c) Cross section of the SiC crystal shown in b).

The red area shows the material which is removed by FIB milling to get a free view on the cross section which can be seen in Fig. 6c). The following discussion is related to the red colored cross section of Fig. 6c).

Two different SiC phases can be seen (④) which are separated by a grain boundary. The interface between the SiC crystal and the silicon bulk is shown by the arrows at ⑤. The typical hexagonal structure which is formed by SiC crystals accounts for a strong chemical bonding to the silicon bulk. Thus these kinds of impurities can only be removed by a long CP which releases the particles from the bulk. Due to the higher mechanical stability of SiC, the crystal is not removed as fast as the bulk silicon by FIB. This can be seen at ⑥. Here the SiC crystal is supposed to have a deep extension into the silicon bulk. Detailed characterization and the depth of the rootage in the bulk are subject of further research.

On solar cell level the SiC inclusions are supposed to lead to shunts in the emitter of the cell. This can be recognized by the hot spots of illuminated lock-in thermography images [12]. Thus a reduction of the SiC crystal density on the wafer surface by adjusting casting material should lead to RST wafers with a higher material quality.

6 CONCLUSION

RST wafers are a competitive alternative to block-cast multicrystalline silicon. They can be produced fast, energy- and material-effective since no energy-consuming ingot growth or wire sawing is needed. Lifetime samples have been processed on different RST wafers and characterized by QSSPC and PL. Wafers with higher base resistivity show a tendency to higher lifetimes. The burn-off temperature, the position at the ribbon and the quality of the carbon carrier also have an influence on $\tau_{eff.}$ Spatially resolved lifetime calibrated PL maps reveal an inhomogeneous distribution of the minority-carrier lifetimes over the whole sample. The distribution of lifetime can be broadened and shifted to higher values by hydrogen diffusing in the sample during firing of a SiN_x:H_y layer. Many defects can be passivated by H.

Grain boundaries which are observed by optical microscopy after a defect etch on the RST surface are not the limiting factor for τ_{eff}. Disturbed crystal growth and high defect densities in some grains might be the main reason for reduced τ_{eff}. EBSD measurements have been performed to identify the CSL grain boundary type. The predominant type is found to be Σ3. Σ9, Σ27a and higher order GB types are found at the interface of different Σ3 orientations. These are recombination active and cannot be fully passivated by H. SEM and EDX measurements show different types of SiC particles on the silicon surface as residuals of the carbon carrier. The particles can be the starting point of disturbed crystal growth. Some are deeply ingrained in the silicon bulk by a reaction of the molten silicon and the carbon carrier during ribbon casting. These kinds of particles can lead to electrical shunts of RST solar cells.

7 ACKNOWLEDGEMENTS

The authors would like to thank Solarforce (France) for providing the RST wafer material and A. Hammud for EDX measurement support. Part of this work is supported

by the French government “Investment for the future” program supervised by the ADEME (DEMOS project). The content of this publication is the responsibility of the authors.

8 REFERENCES

[1] C. Belouet, J. Cryst. Growth 82 (1987) 110.
[2] G. Hahn, S. Seren, M. Kaes, A. Schonecker, J.P. Kalejs, C. Dube, A. Grenko, C. Belouet, Proc. 4th WCPEC (2006) 972.
[3] R.A. Sinton, A. Cuevas, Appl. Phys. Lett. 69(17) (1996) 2510.
[4] T. Trupke, R.A. Bardos, M.C. Schubert, W. Warta, Appl. Phys. Lett. 89, (2006) 44107.
[5] B.L. Sopori, ECS Trans. 18(1) (2009) 1049.
[6] B.L. Sopori, J. Electrochem. Soc. 131 (1984) 667.
[7] S. Herlufsen, J. Schmidt, D. Hinken, K. Bothe, R. Brendel, Phys. Stat. Sol. (RRL) 2(6) (2008) 245.
[8] F. Humphreys, J. Mat. Sci., 36(16) (2001) 3833.
[9] G. Hahn, A. Schönecker, J. Phys.: Condens. Matter 16(50) (2004) R1615.
[10] A. Gervais, R. Sharko, T. Moudda-Azzem, C. Belouet, J. Cryst. Growth 82 (1987) 209.
[11] R.O. Bell, J.P. Kalejs, J Mater Res 13 (1998) 2732.
[12] P. Keller, F. de Moro, S. Seren, G. Hahn, Energy Procedia 38 (2013) 576.
[13] G. Hahn, M. Käs, B. Herzog, Sol. State Phen. 156-158 (2010) 343.
[14] H. Wagner, M. Müller, G. Fischer, P.P. Altermatt, Proc. 27th EUPVSEC (2012) 1213.
[15] M. Bertoni, S. Hudelson, B. Newman, D. Fenning, H. Dekkers, E. Cornagliotti, A. Zuschlag, G. Micard, G. Hahn, G. Coletti, B. Lai, T. Buonassisi, Prog. Photovolt.: Res. Appl., 19(2) (2011) 187.
[16] J. Chen, D. Yang, Z. Xi, T. Sekiguchi, Physica B: Cond. Matt. 364 (2005) 162.
[17] M. Rinio, M. Kaes, G. Hahn, D. Borchert, Proc. 21st EUPVSEC (2006) 684.
[18] J. Junge, A. Herguth, S. Seren, G. Hahn, Proc. 24th EUPVSEC (2009) 1131.
[19] P. Karzel, M. Ackermann, L. Gröner, C. Reimann, G. Hahn, Proc. 28th EUPVSEC (2013), to be published.
[20] C.V. Hari Rao, H.E. Bates, K.V. Ravi, J. Appl. Phys. 47(6) (1976) 2614.